Crystal Morphology and Structure of the β-Form of Isotactic Polypropylene Under Supercooled Extrusion

Bin Zhang, Jingbo Chen, Xiaoli Zhang, Changyu Shen

College of Material Science and Engineering, National Engineer Research Center for Advanced Polymer Processing Technology, Zhengzhou University, Zhengzhou 450002, People's Republic of China

Received 19 October 2009; accepted 7 September 2010
DOI 10.1002/app.33372
Published online 22 February 2011 in Wiley Online Library (wileyonlinelibrary.com).

ABSTRACT: A supercooled melt of isotactic polypropylene (iPP) was extruded through a capillary die. Polarized light microscopy (PLM), wide-angle X-ray diffraction (WAXD), and differential scanning calorimetry (DSC) were used to investigate the effects of the relatively weak wall shear stress (σ_w), extrusion temperature (T_e), and crystallization temperature (T_c) on the structure and morphology of β-form isotactic polypropylene (β-iPP). β-cylindrites crystals could be observed by PLM in the extruded specimen even at a lower σ_w's (0.020 MPa), and the β-iPP content increased with decreasing T_e. Under a given T_e of 150°C, the increase in σ_w positively influenced the β-iPP content. The DSC and WAXD results indicate that the total crystallinity and β-iPP content increased when T_c was set from 105 to 125°C; the other experimental parameters were kept on the same level. Although T_c was above 125°C, the β-iPP content obviously decreased, and the total crystallinity continued to increase. On the basis of the influences of σ_w, T_e, and T_c on the β-iPP crystal morphology and structure, a modified model is proposed to explain the growing of shear-induced β-iPP nucleation. J Appl Polym Sci 120: 3255–3264, 2011

Key words: crystal structures; extrusion; melt; poly (propylene) (PP)

INTRODUCTION

In most industrial processing operations (e.g., extrusion, injection molding, blow molding), polymer melts are subjected to different types of flow before crystallization.[1] The structure and morphology of the resulting crystals are strongly influenced by the applied flow conditions.[2–6] It is possible to control and predict the final morphologies and properties of semicrystalline polymers by controlling different shear flow parameters.[7–15] It is well known that isotactic polypropylene (iPP) exhibits pronounced polymorphic crystalline modifications, which are designated as α-form (α-iPP), β-form (β-iPP), and γ-form (γ-iPP).[16–18] In addition, three types of α spherulites and two types of β-spherulites might be formed, depending on different crystallization temperature's (T_c's); these include α_I (radial spherulite), α_{II} (negative radial spherulite), α_m (mixed radial), and β_{III} (negative radial spherulite), and β_{IV} (negative ringed spherulite).[19,20] In quiescent conditions, iPP can crystallize essentially into spherulitic structures. As β-iPP has many performance characteristics, such as a high toughness, drawability, and thermal deformation temperature, many research groups have focused their interest on β-iPP. Furthermore, even a weak shear stress pressed on molten iPP can lead to a cylindrite crystal structure.[21] β-iPP is thermodynamically metastable. The doping of certain nucleating agents[22–24] is one of the most effective and accessible method for obtaining a higher β-iPP content.

Various laboratory techniques have been used to study the crystallization of a supercooled melt under or after shear: fiber pullout, rheo-X-ray diffraction, die extrusion, and so on. Fiber pullout[25–28] has proven to be suitable for studying the nucleation mechanism of cylindrite crystalline in the iPP supercooled melt after shear. It was suggested that the shear effect leads to the development of α-row nuclei along the fiber and on the surface of such α-row nuclei, α-to-β growing transitions, or α,β-bifurcation. In another case, Yan et al.[29] applied homogeneous fiber/matrix composites of iPP to study the effect of the orientation structure on the β-iPP crystals of its supercooled melt. It was proposed that the molten higher oriented iPP fiber played the same role as that of the α-row nuclei generated by fiber pulling during the process of crystallization. Rheo-small-angle X-ray scattering and rheo-wide-angle X-ray diffraction were applied to relevant studies by Hsiao and coworkers[30,31] to probe the shear-induced precursor in certain supercooled melts.

Correspondence to: J. Chen (chenjb@zzu.edu.cn).
Contract grant sponsor: National Natural Science Foundation of China; contract grant numbers: 10772164, 10590352.

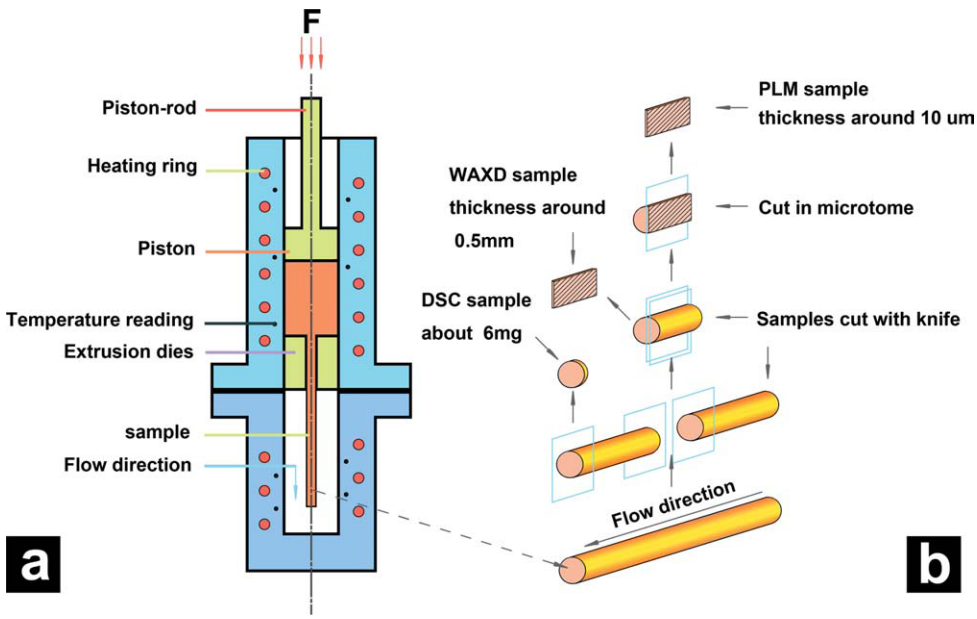

Figure 1 Extrusion and preparation of the shear-induced crystalline samples: (a) sample extrusion from the die and (b) preparation of the specimen. Figure 1(a) shows the Force (F) direction. [Color figure can be viewed in the online issue, which is available at wileyonlinelibrary.com.]

Additionally, several industrial apparatuses, such as injection molding,[32] shear-controlled orientation in injection molding,[33–35] vibration-assisted injection,[36] and the push–pull processing technique,[37,38] were used to generate higher shear stresses and strain rates, which were close to that of real processing. Farah and Bretas[39] prepared shear-induced crystallization samples through extruding an iPP melt from the slit die of a twin-screw extruder. The shear-induced crystalline layers developed in the slit die were observed. To avoid the effect of premechanical history on the iPP melt, Peters et al.[40] introduced a capillary rheometer to drive the melt through the slit die.

In other studies, the formation of the precursor and the crystallization structure under different shear flows have been given special concern.[7,41–50] We are more interested in the β-iPP nuclei formation conditions and the related morphology and structure of β-iPP. Different supercooled extrusion shear strength conditions measured between laboratory and industrial techniques were designed. The combined influences of the wall shear stress (σ_w), extrusion temperature (T_e), and crystallization temperature (T_c) on the development of the supermolecular structure of β-iPP were examined in this study. Relevant results were explicated by the knowledge of flow-induced precursor theory.[30,31]

EXPERIMENTAL

Materials and sample preparation

The iPP (F401, GB-2401), with a melt flow index of 3.0 g/10 min, an isotacticity index of 0.96, and a melting temperature (T_m) of 170°C, used in this study was produced by Yangzi Petroleum and Chemical Corp. (Nanjing, China). The granular iPP materials were used without any further treatment.

To obtain shear-induced crystallization samples under different shear conditions, a homemade rheometer was used, as shown in Figure 1(a). The diameter of the capillary die was 2.00 mm, with a length of 8.00 mm. Because of outlet expansion and solidification contraction, the final sample diameters were measured to be between 2.30 and 3.60 mm after cooling. At the same σ_w of 0.090 MPa, the supercooled T_e's (below the nominal T_m) were set at 140, 145, 150, 155, 160, and 165°C. The temperature stability was maintained within ±0.3°C.

Before shearing, the iPP materials were subjected to a thermal treatment to erase the possible effects of thermal or mechanical history before further measurements. The thermomechanical protocol adopted for the shear-induced crystallization experiments is described in Figure 2:

1. We heated the sample from room temperature to 210°C at a rate of 10°C/min.
2. We held the temperature (T) at 210°C (T_a) for 10 min to erase the thermomechanical prehistory.
3. The sample was cooled at 4°C/min to T_e.
4. The temperature was held at T_e for 10 min. (T_{eh} and T_{el} are the maximum and minimum T_e, respectively)
5. The sample was extruded at T_e, and then, the extruded sample was cooled to T_c. (t_0 and t_s are the initial time and final time of extrusion process, respectively)
6. The sample was then cooled to room temperature.

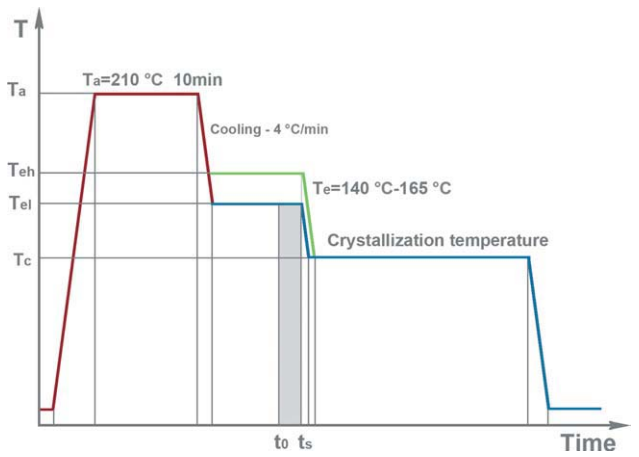

Figure 2 Experimental protocol for the shear-enhanced crystallization experiments. [Color figure can be viewed in the online issue, which is available at wileyonlinelibrary.com.]

To measure the influence of different σ_w's at the same T_e (150°C) on the supercooled melt, the values of σ_w were set at 0.020, 0.045, 0.090, and 0.130 MPa. The corresponding characteristic shear rates ($\dot{\gamma}$'s), ranging from 0.81 to 41.5 s^{-1}, were calculated from $\dot{\gamma} = 4Q/\pi R^2$ where Q is the volume flux of polymer melt and R is the radius of the capillary die.

Polarized optical microscopy (PLM)

Figure 1(b) shows the sample preparation procedure. Each section had a length of 10.00 mm, which was microtomed by a glass knife fixed on a RMC Powertome XL ultramicrotome (RMC, Tucson, Arizona, USA) to produce films with a thickness of 10 μm along the flow direction. For morphological observation, an Olympus BX-2 optical microscope (Olympus, Tokyo, Japan) at crossed polarizer mode was used in this study.

Differential scanning calorimetry (DSC)

Thermal analysis was performed under an ultra-high-purity nitrogen atmosphere with an MDSC-2920TA thermal analyzer (TA Instruments, DE, USA) in standard mode. Indium of high purity was used to calibrate the DSC temperature and enthalpy scales. Samples of about 6 mg were cut from the cross section of the extrudant. To monitor the melting behavior, samples were heated to 200°C at a heating rate of 10°C/min. The percentage of β-iPP crystals (Φ_β) was obtained from Eq. (1). The crystallinity ($X_{i,i=\alpha,\beta}$) of the α-form (X_α) and the crystallinity of the β-form (X_β) were calculated separately according to Eq. (2). The total crystallinity derived from the DSC data (X_C^{DSC}) was derived from Eq. (3):

$$\Phi_\beta = \frac{X_\beta}{X_\alpha + X_\beta} \times 100\% \quad (1)$$

$$X_i = \frac{\Delta H_i}{\Delta H_i^0} \times 100\% \quad (2)$$

$$X_C^{DSC} = X_\alpha + X_\beta \quad (3)$$

In Eq. (2), ΔH_i is the calibrated specific fusion heat of the α-form or β-form and ΔH_i^0 is the standard fusion heat of the α-iPP and β-iPP crystals, which were 178 and 170 J/g, respectively:[51]

$$\Delta H_\beta = A \times \Delta H_\beta^* \quad (4)$$

$$A = \left[1 - \frac{h_2}{h_1}\right]^{0.6} \quad (5)$$

$$\Delta H_\alpha = \Delta H - \Delta H_\beta \quad (6)$$

The total fusion heat (ΔH) was integrated from 90 to 180°C on the DSC melting curves. A vertical line was drawn through the minimum between the α- and β-fusion peaks, and ΔH was divided into the β component (ΔH_β^*) and α component (ΔH_α^*). Because the less perfect α crystals melted before the maximum point during heating and contributed to ΔH_β^*, we approximated the true value of β-fusion heat (ΔH_β) by multiplying ΔH_β^* by a calibration factor (A).[52] In these calculations, h_1 and h_2 are the heights from the base line to the β-fusion peak and minimum point, respectively (see Fig. 3).

Because the total DSC curves of the extrusion sample exhibited both α- and β-fusion peaks, the relative amounts of α- and β-iPP crystals were evaluated by the method of Li and coworkers.[52,53] X_C^{DSC} and Φ_β of the extruded specimens were measured with DSC, and the results are summarized in Figures 8, 11, and 14 (shown later).

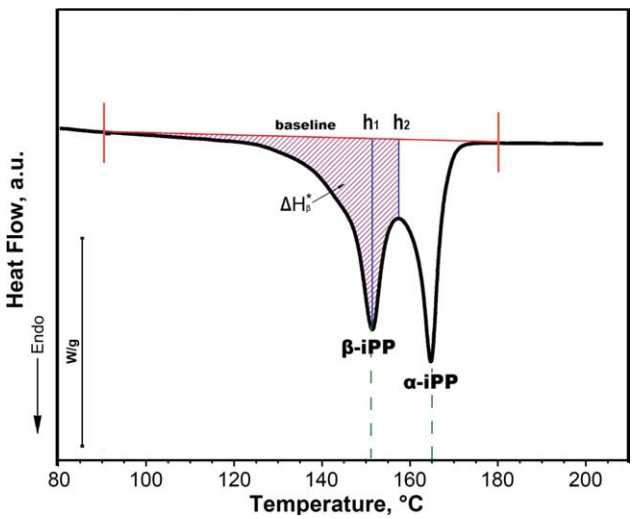

Figure 3 DSC melting curves of iPP containing β-form crystals. [Color figure can be viewed in the online issue, which is available at wileyonlinelibrary.com.]

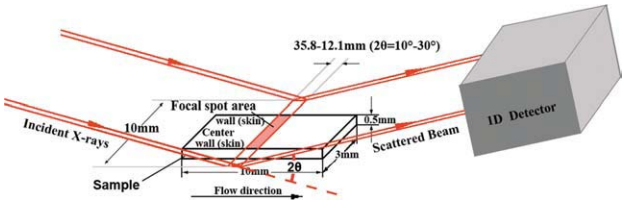

Figure 4 Schematic diagram of the one-dimensional (1D) WAXD experiment. [Color figure can be viewed in the online issue, which is available at wileyonlinelibrary.com.]

Wide-angle X-ray diffraction (WAXD)

The WAXD measurements were carried out on a Rigaku D/max-3B diffractometer (Rigaku Co, Tokyo, Japan) equipped with a graphite monochromator and with Cu Kα radiation. Intensity data were collected in the reflection mode (see Fig. 4). The equipment was operated at 35 kV and 30 mA with a scan range between 10 and 30°. In Eq. (7), The total crystallinity derived from the WAXD data (X_C^{WAXD}) was expressed as the mass fraction of the crystalline phase and was determined from the WAXD patterns on the basis of the ratio of the integrated intensity under the crystalline peaks (A_c) to the integrated total intensities: $A = A_c + A_a$, where A_a is the integrated intensity under the amorphous halo:

$$X_C^{WAXD} = \frac{A_c}{A_c + A_a} \times 100\% \quad (7)$$

$$K_\beta = \frac{I_{\beta 1}}{I_{\beta 1} + I_{\alpha 1} + I_{\alpha 2} + I_{\alpha 3}} \quad (8)$$

According to Tuner-Jones,[54] the relative amount of the β-form (K_β) can be calculated with Eq. (8), in which $I_{\beta 1}$ is the peak intensity due to the β{3 0 0} plane at a diffraction angle (2θ) of 16° and $I_{\alpha 1}$, $I_{\alpha 2}$, and $I_{\alpha 3}$ are the diffraction intensities of the three stronger peaks due to the α{1 1 0}, α{0 4 0}, and α{1 3 0} planes located at 2θ = 14.1, 16.9, and 18.8°, respectively.

For all of the WAXD profiles, the amorphous background was extracted, and then, the peaks were deconvoluted with Materials Data Jade 5.0 software (Materials Data Inc, Livermore, CA, USA). X_C^{WAXD} and K_β were measured with WAXD, and the results are summarized in Figures 8, 11, and 14 (shown later). The detector and specimen rotated simultaneously such that the angle between the beam and the specimen surface was the same as the angle between the specimen surface and the detector. In this 2θ mode of operation, the diffraction planes were parallel to the specimen surface and the flow direction [the scattering angle (2θ) is the angle between the scattered and incident directions].

RESULTS AND DISCUSSION

Effect of T_e on the crystal structure and morphology of the iPP supercooled melt

Figure 5 shows the cross section of iPP extrudant prepared at a σ_w of 0.090 MPa and T_e's of 140°C

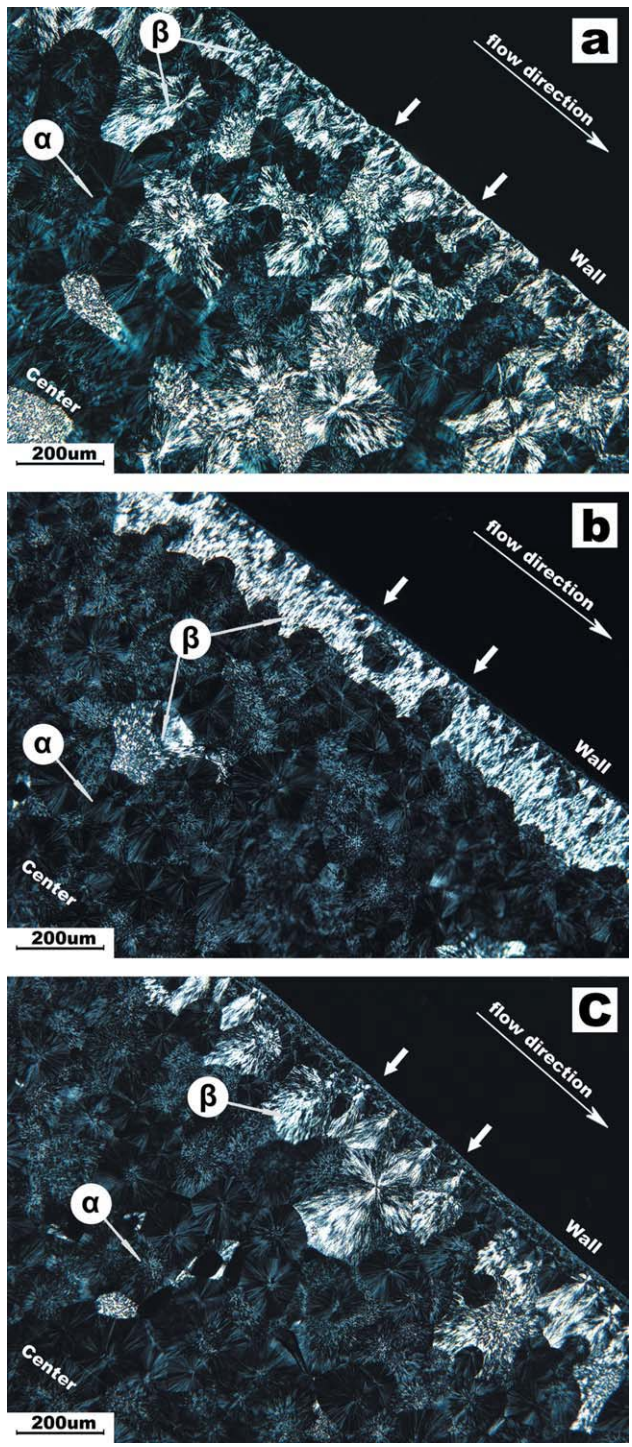

Figure 5 Optical micrographs of the iPP samples subjected to extrusion with σ_w = 0.090 MPa and various T_e values: (a) 140, (b) 155, and (c) 165°C. [Color figure can be viewed in the online issue, which is available at wileyonlinelibrary.com.]

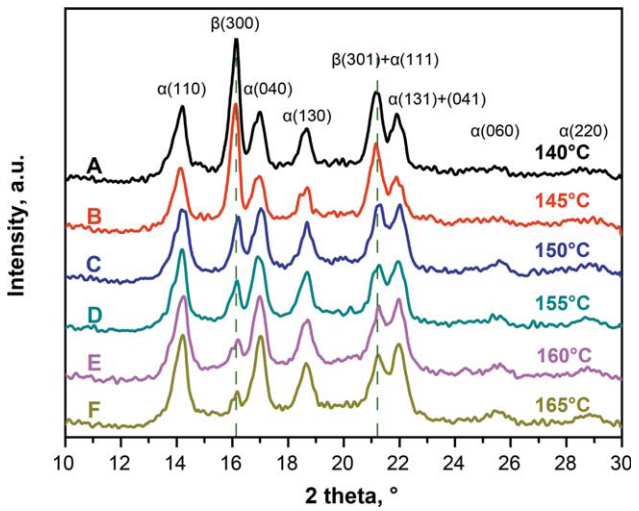

Figure 6 WAXD patterns of samples subjected to extrusion with a constant σ_w of 0.090 MPa and various T_e's. [Color figure can be viewed in the online issue, which is available at wileyonlinelibrary.com.]

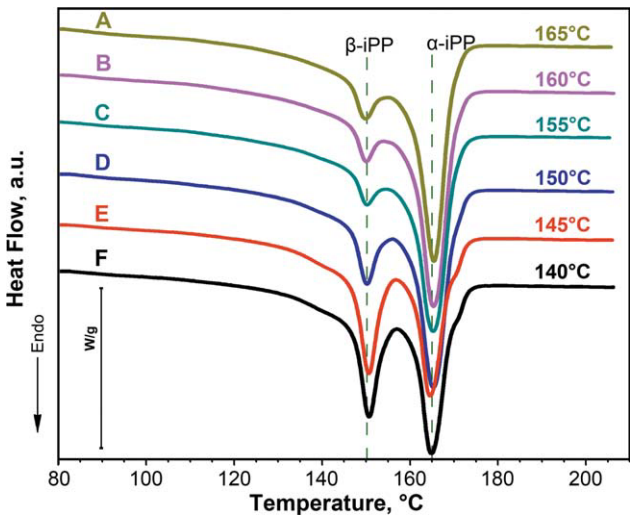

Figure 7 DSC thermograms of samples subjected to extrusion with a constant σ_w of 0.090 MPa and various T_e. W/g is heat-flow unit (W/g = watt/gramme). [Color figure can be viewed in the online issue, which is available at wileyonlinelibrary.com.]

[Fig. 5(a)], 155°C [Fig. 5(b)], and 165°C [Fig. 5(c)] and then rapidly cooled to 105°C for 1 h. The skin–core structure[55,56] is shown in Figure 5, from which two distinct regions were observed: the row-nucleated cylindritic region and the spherulite region. In the row-nucleated cylindritic region, the β-iPP cylindrite crystals, about 100 μm in radius, were found near the wall, and the density of the β-iPP cylindrite nuclei decreased rapidly with increasing T_e. In the spherulite region, spherulites with a diameter of about 100–200 μm were dominant. The bright regions are β-crystal forms, and the dark ones are α-crystal forms. However, it was also observed in this region that the number of β-iPP spherulites in Figure 5(a) was comparatively greater than that in Figure 5(b,c).

Figure 6 shows the WAXD patterns of the iPP samples shown in Figure 5. It is well known that the important characteristics of WAXD for the β-form can be found at 2θ's of 16° {3 0 0} and 21.2° {3 0 1}, and among them, the peak at 16° implies the existence of a thimbleful of β-form. The results also suggest that the peaks at 16° gradually weakened with increasing T_e; this was in agreement with the trend observed in the optical micrographs.

The α-form of the iPP extrudant (T_e = 140°C, T_c = 105°C, and σ_w = 0.090 MPa) had a monoclinic unit cell with parameters (a, b, c, β) a = 6.60 Å, b = 20.77 Å, c = 6.54 Å, and β = 98.71°. On the other hand, the β-form of the iPP extrudant had a trigonal unit cell with parameters $a = b$ = 18.99 Å, c = 6.51 Å, α = β = 90°, γ = 60°, and so on. The structural parameters obtained for the α-iPP phase and β-iPP phase were quite similar to those proposed by Turner-Jones[54] and Samuels and Yee,[17] respectively. The lattice parameters of α-iPP and β-iPP were insensitive to the weak shear flow.

For comparison, DSC was used to characterize the contents of the β-form crystals of the same samples. The melting curves of the iPP samples that were subjected to extrusion with a constant σ_w of 0.090 MPa and various T_e's are presented in Figure 7. The peaks around 166 and 151°C were attributed to the melting of α-iPP and β-iPP, respectively.[57]

Φ_β and K_β, calculated from eqs. (1) and (5), gradually decreased as T_e increased, but surprisingly, X_C^{DSC} and X_C^{WAXD} remained almost invariant. The data presented in Figure 8 demonstrate that K_β decreased from 44 to 10 wt % (a reduction of 34%)

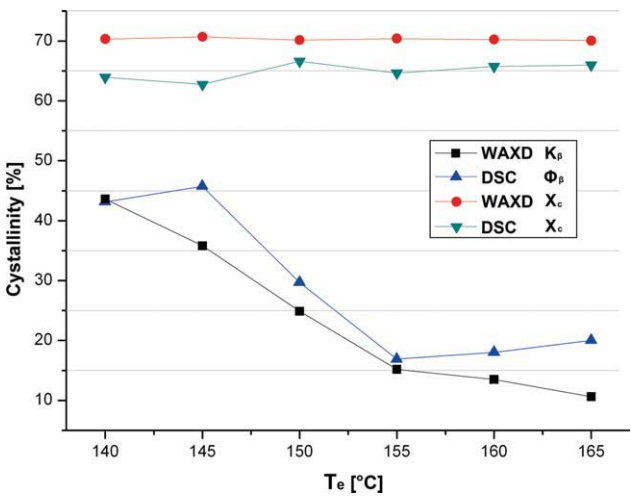

Figure 8 Dependence of the total crystallinity (X_c) and β-iPP content on the various T_e's applied, as derived from DSC and WAXD data. [Color figure can be viewed in the online issue, which is available at wileyonlinelibrary.com.]

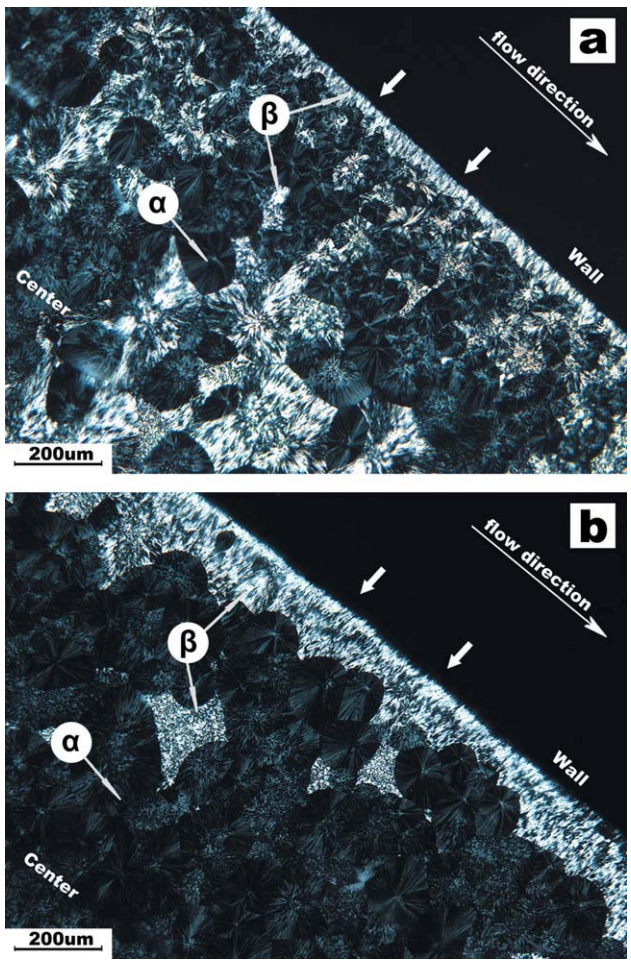

Figure 9 Optical micrographs of iPP samples subjected to extrusion with T_e = 150°C and various σ_w's: (a) 0.090 and (b) 0.045 MPa. [Color figure can be viewed in the online issue, which is available at wileyonlinelibrary.com.]

when the applied T_e increased from 140 to 165°C. Meanwhile, Φ_β decreased from 43 to 20 wt % (a reduction of 23%). Because of the different mechanisms, the two sets of values of β-iPP content, counted from the DSC and WAXD methods, did not coincide, but both could illuminate the decreasing β-iPP content with increasing T_e. Because of the different methods of computation, the absolute values for the total crystallinity were impossible to obtain, and only approximate values could be obtained. However, in general, these approximate crystallinity values were still helpful in understanding the law of crystallinity change.

Effect of σ_w on the crystal structure and morphology of the iPP supercooled melt

Figure 9 gives the skin–core structure of the iPP samples with a given T_e and various σ_w's. When Figure 9(a) was compared with Figure 9(b), we found β-iPP cylindrite crystals in the row-nucleated cylindritic region in both figures. In the spherulite

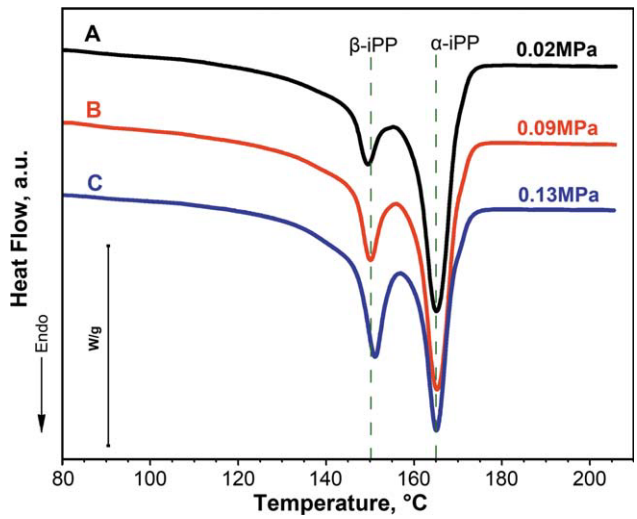

Figure 10 DSC thermograms of samples subjected to extrusion with a constant T_e of 150°C and various σ_w's. [Color figure can be viewed in the online issue, which is available at wileyonlinelibrary.com.]

region, as shown in Figure 9(b), crystals almost composed of pure α spherulites were observed. However, as shown in Figure 9(a), a great number of larger β spherulites were identified. The melting curves of the iPP samples that were subjected to extrusion with a constant T_e of 150°C and various σ_w's are presented in Figure 10.

As shown in Figure 11, Φ_β, K_β, X_C^{DSC}, and X_C^{WAXD} of the extrudant treated by various σ_w's were counted. Φ_β and K_β gradually increased, and X_C^{DSC} and X_C^{WAXD} remained almost invariant; this depended strongly on the increase in σ_w. K_β decreased from 51 to 12 wt % (a reduction of 39%) when the applied σ_w decreased from 0.130 to 0.020 MPa. Meanwhile, Φ_β decreased from 40 to 25 wt %

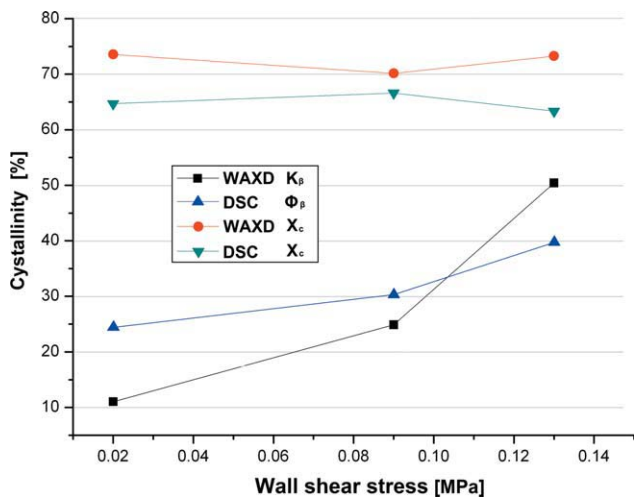

Figure 11 Dependence of the total crystallinity (X_c) and β-iPP content with T_e = 150°C and various σ_w's applied, derived from the DSC and WAXD data. [Color figure can be viewed in the online issue, which is available at wileyonlinelibrary.com.]

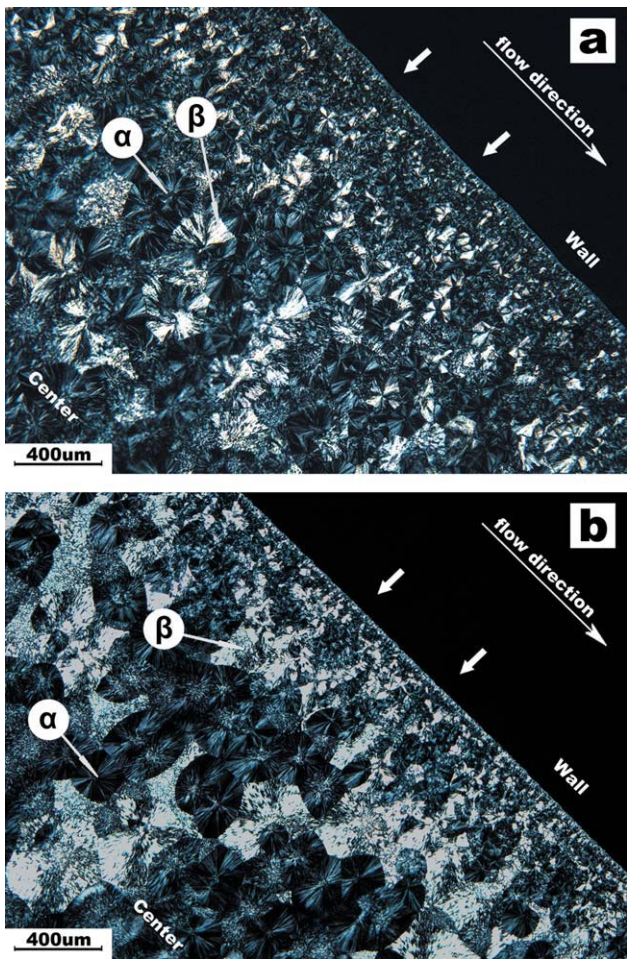

Figure 12 Optical micrographs of iPP samples subjected to extrusion with T_e = 145°C and σ_w = 0.090 MPa crystallized at T_c's of (a) 135 and (b) 125°C for 60 min. [Color figure can be viewed in the online issue, which is available at wileyonlinelibrary.com.]

(a reduction of 25%). This showed that the DSC and WAXD results were in agreement with the trend observed by the optical micrographs (see Fig. 9). Similar behavior was found in recent studies.[58–60]

Effect of T_c on the crystal structure and morphology of the iPP supercooled melt

Figure 12 shows the influence of different T_c's on extrusion samples that were extruded with a σ_w of 0.090 MPa at a T_e of 145°C and then held for 1 h at different T_c's. Two types of β-iPP spherulites are shown in Figure 12: the negative radial β_{III}-iPP [Fig. 12(a)] and the negative banded β_{IV}-iPP [Fig. 12(b)], as defined by Padden and Keith.[57] As shown in Figure 12(b), β-iPP cylindrites were observed near the wall. However, it was hard to find them in the same region in Figure 12(a).

Figure 13 shows DSC thermograms of samples that were extruded with a σ_w of 0.090 MPa at a T_e of 145°C and then held for 1 h at different T_c's. Notice-

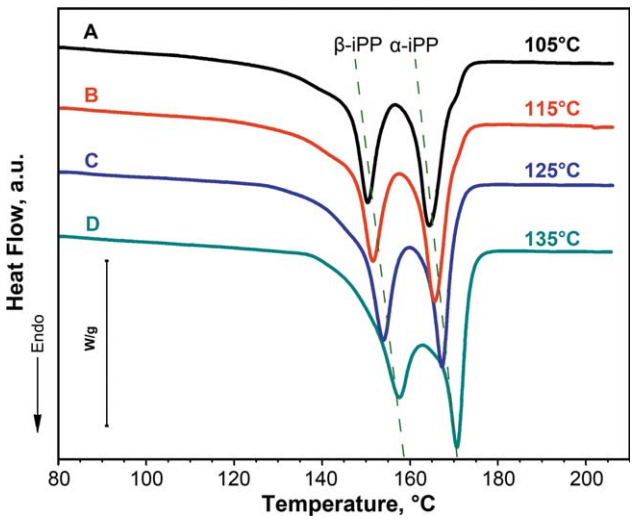

Figure 13 DSC thermograms of samples subjected to extrusion with T_e = 145°C and σ_w = 0.090 MPa crystallized at various T_c's. [Color figure can be viewed in the online issue, which is available at wileyonlinelibrary.com.]

ably, the T_m's of both the α-form and β-form crystals in the extrudant consistently shifted to higher temperatures when the applied T_c increased from 105 to 135°C (see Fig. 13). This may have been due to the increased perfection of the crystals when the crystallization was conducted at higher T_c's.[61,62]

The effect of T_c on Φ_β, K_β, X_C^{DSC}, and X_C^{WAXD} is shown in Figure 14. The DSC and WAXD results indicate that the total crystallinity and β-iPP content increased when T_c was set from 105 to 125°C, with a constant σ_w of 0.090 MPa and a T_e of 145°C. When T_c was above 125°C, the β-iPP content decreased obviously, and the total crystallinity continued to increase. On the other hand, we believe that the final

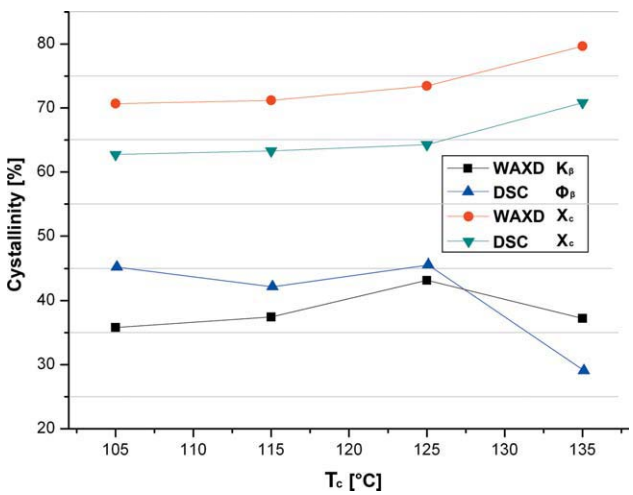

Figure 14 Dependence of the total crystallinity (X_c) and β-iPP content with T_e = 145°C, σ_w = 0.090 MPa, and various T_c's applied, derived from the DSC and WAXD data. [Color figure can be viewed in the online issue, which is available at wileyonlinelibrary.com.]

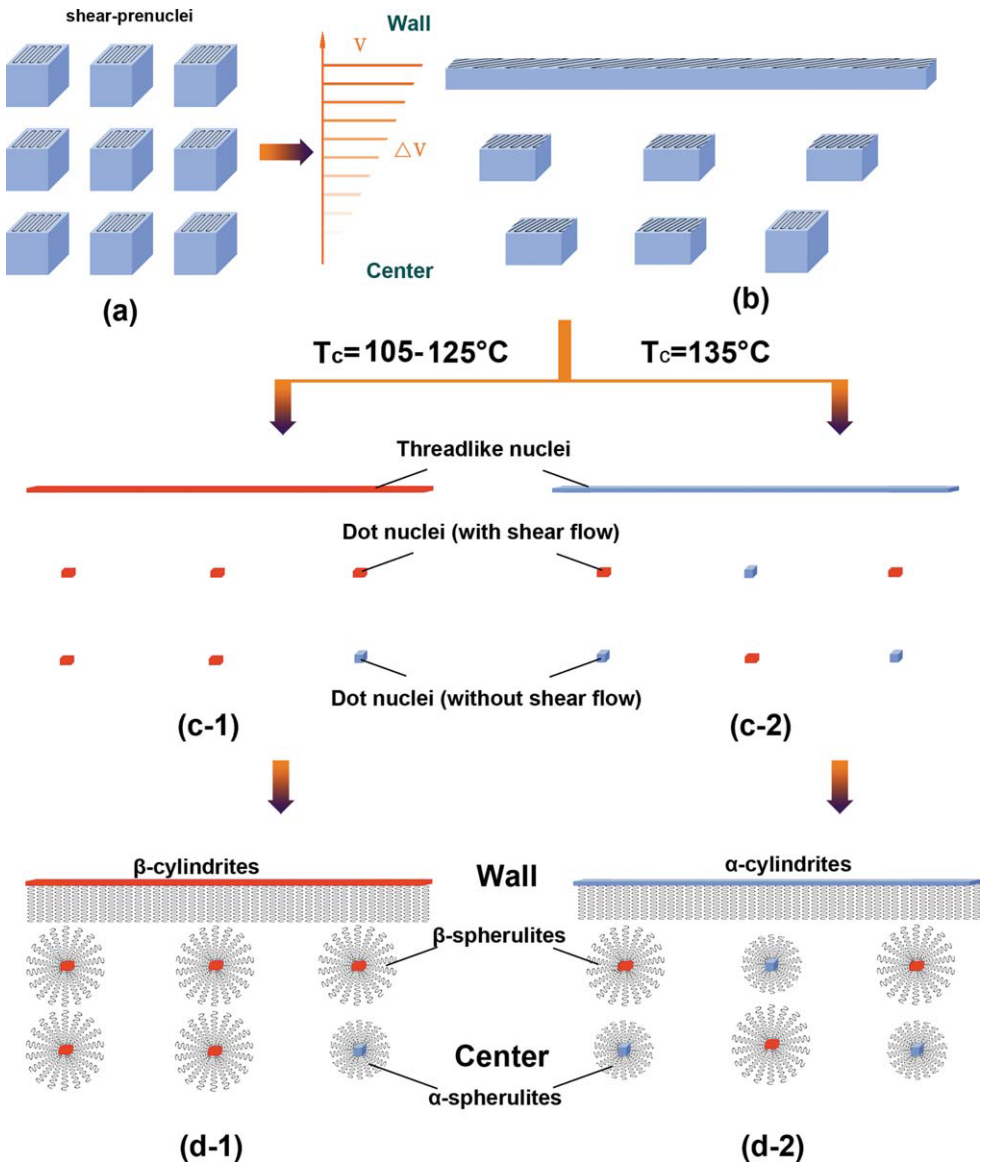

Figure 15 Schematic model of the morphological development of shear prenuclei during the flow-induced crystallization of the iPP supercooled melt. V = velocity; ΔV = velocity difference. [Color figure can be viewed in the online issue, which is available at wileyonlinelibrary.com.]

crystal morphology and structure were changed after the relaxation of the oriented structure at higher T_c's; this may have dominated the formation of β-iPP.

According to these experimental results obtained at different values of σ_w, T_e and T_c, we suggest a schematic model of three steps to describe the development of the flow-induced crystallization of the iPP supercooled melt shown in Figure 15:

1. As shown in Figure 15(a), some partially ordered molecular bundles existing in the iPP supercooled quiescent melt acted as shear prenuclei during the course of shearing.
2. Threadlike and dot nuclei (under shear flow) came from shear prenuclei, which were stretched parallel to flow direction, as demonstrated in Figure 15(b).
3. As shown in Figure 15(c-2), these threadlike and dot nuclei (under shear flow) were easily relaxed at higher T_c (marked in blue). We suggest that the higher T_c of the iPP extrudant inhibited the formation of β-iPP; this was actually observed in this case.
4. An adjacent chain was adsorbed to these ordered structures during the process of crystallization after extrusion, as shown in Figure 15 (d-1) and Figure 15(d-2).

Because threadlike and dot nuclei could crystallize at much higher temperatures compared with the

homogeneous nucleation,[20] the well-developed β-cylindrite and β-spherulite crystals shown in Figure 15(d-1) were easily understood. The dot nuclei fell into two broad categories: shear-induced dot nuclei and quiescent dot nuclei. Shear-induced dot nuclei doubtlessly led to a tendency to form β-spherulite crystals. The resulting morphology consisted of β-spherulite, α-spherulite, and β-cylindrite crystals. The description of this model was consistent with simulation works carried out in recent studies.[63–65]

CONCLUSIONS

By detecting iPP extruded samples prepared at different values of σ_w, T_e, and T_c, we drew the following conclusions:

1. β-cylindrites could found near the wall in almost all extrudants, and the density of the β-cylindrite nuclei decreased rapidly with increasing T_e, although in the core region, only under higher σ_w's could β-spherulites be observed.
2. Compared with the gradually decreasing β-iPP content, when T_e increased, the total crystallinity remained almost invariant.
3. With increasing σ_w, the β-iPP content gradually increased, but the total crystallinity still remained invariant.
4. With T_c climbing from 105 to 125°C, the total crystallinity and β-iPP content positively changed accordingly; above125°C, the β-iPP content decreased obviously, whereas the total crystallinity increased obviously.

From these results, we suggest that some partially ordered molecular bundles remained in the iPP quiescent supercooled melt. Those above a critical size could orient under flow and form crystal nuclei of β-cylindrite and β-spherulite crystals, known as *shear prenuclei*. The size of the shear prenuclei may have been influenced by the supercooled T_e.

References

1. Lee, O.; Kamal, M. R. Polym Eng Sci 1999, 39, 236.
2. Lellinger, D.; Floudas, G.; Alig, I. Polymer 2003, 44, 5759.
3. Watanabe, K.; Suzuki, T.; Masubuchi, Y.; Taniguchi, T.; Takimoto, J.; Koyama, K. Polymer 2003, 44, 5843.
4. Lieberwirth, I.; Loos, J.; Petermann, J.; Keller, A. J Polym Sci Part B: Polym Phys 2000, 38, 1183.
5. Kumaraswamy, G.; Kornfield, J. A.; Yeh, F.; Hsiao, B. S. Macromolecules 2002, 35, 1762.
6. Kumaraswamy, G.; Issaian, A. M.; Kornfield, J. A. Macromolecules 1999, 32, 7537.
7. Seki, M.; Thurman, D. W.; Oberhauser, J. P.; Kornfield, J. A. Macromolecules 2002, 35, 2583.
8. Coppola, S.; Balzano, L.; Gioffredi, P. L.; Maffettone, P. L.; Grizzuti, N. P. Polymer 2004, 45, 3249.
9. Balzano, L.; Rastogi, S.; Peters, G. W. M. Macromolecules 2008, 41, 399.
10. Jay, F.; Haudin, J. M.; Monasse, B. J Mater Sci 1999, 34, 2089.
11. Peron, B.; Lowe, A.; Baillie, C. Compos A 1996, 27, 839.
12. Devaux, E.; Chabert, B. Polym Commun 1991, 32, 464.
13. Monasse, B. J Mater Sci 1992, 27, 6047.
14. Duplay, C.; Monasse, B.; Haudin, J.; Costa, J. Polym Int 1999, 48, 320.
15. Haudin, J.; Duplay, C.; Monasse, B.; Costa, J. L. Macromol Symp 2002, 185, 119.
16. Turner-Jones, A.; Cobbold, A. J. J Polym Sci 1968, 6, 539.
17. Samuels, R. J.; Yee, R. Y. J Polym Sci Part A-2: Polym Phys 1972, 10, 385.
18. Bruckner, S.; Meille, S. V. Nature 1989, 340, 455.
19. Varga, J. Angew Makromol Chem 1982, 104, 79.
20. Varga, J. J Mater Sci 1992, 27, 2557.
21. Varga, J. Angew Makromol Chem 1983, 112, 191.
22. Xiao, W. C.; Wu, P. Y.; Feng, J. C. J Appl Polym Sci 2008, 108, 3370.
23. Xiao, W. C.; Wu, P. Y.; Feng, J. C.; Yao, R. Y. J Appl Polym Sci 2009, 111, 1076.
24. Yamaguchi, M.; Fukui, T.; Okamoto, K.; Sasaki, S.; Uchiyama, Y.; Ueoka, C. Polymer 2009, 50, 1497.
25. Varga, J.; Karger-Kocsis, J. J Polym Sci Part B: Polym Phys 1996, 34, 657.
26. Varga, J.; Karger-Kocsis, J. Polymer 1995, 36, 4877.
27. Varga, J. J Macromol Sci Phys 2002, 41, 1121.
28. Sun, X.; Li, H.; Wang, J.; Yan, S. Macromolecules 2006, 39, 8720.
29. Li, H.; Jiang, S.; Wang, J.; Wang, D.; Yan, S. Macromolecules 2003, 36, 2802.
30. Somani, R. H.; Yang, L.; Hsiao, B. S.; Agarwal, P. K.; Fruitwala, H.; Tsou, A. H. Macromolecules 2002, 35, 9096.
31. Agarwal, P. K.; Somani, R. H.; Weng, W. Q.; Mehta, A.; Yang, L.; Ran, S. F.; Liu, L. Z.; Hsiao, B. S. Macromolecules 2003, 36, 5226.
32. Cao, J.; Wang, K.; Cao, W.; Zhang, Q.; Du, R. N.; Fu, Q. J Appl Polym Sci 2009, 112, 1104.
33. Kalay, G.; Bevis, M. J. J Polym Sci Part B: Polym Phys 1997, 35, 265.
34. Liang, S.; Yang, H.; Wang, K.; Zhang, Q.; Du, R.; Fu, Q. Acta Mater 2008, 56, 50.
35. Liang, S.; Wang, K.; Tang, C.; Zhang, Q.; Du, R.; Fu, Q. J Chem Phys 2008, 128, 174902.
36. Tom, A. M.; Kikuchi, A.; Coulter, J. P. J Mater Process Manuf Sci 2000, 8, 141.
37. Wang, K.; Guo, M.; Zhao, D.; Zhang, Q.; Du, R.; Fu, Q.; Dong, X.; Han, C. C. Polymer 2006, 47, 8374.
38. Guo, M.; Yang, H.; Tan, H.; Wang, C.; Zhang, Q.; Du, R.; Fu, Q. Macromol Mater Eng 2006, 291, 239.
39. Farah, M.; Bretas, R. E. S. J Appl Polym Sci 2004, 91, 3528.
40. Housmans, J. W.; Gahleitner, M.; Peters, G. W. M.; Meijer, H. E. H. Polymer 2009, 50, 2304.
41. Somani, R. H.; Hsiao, B. S.; Nogales, A.; Srinivas, S.; Tsou, A. H.; Sics, I.; Balta-Calleja, F. J.; Ezquerra, T. A. Macromolecules 2000, 33, 9385.
42. Jerschow, P.; Janeschitz-Kriegl, H. Int Polym Process 1997, 12, 72.
43. Zhang, W.; Martins, J. A. Polymer 2007, 48, 6215.
44. Sherwood, C.; Price, F.; Stein, R. J Polym Sci Polym Symp 1978, 63, 77.
45. Geng, Y.; Wang, G.; Cong, Y.; Bai, L. G.; Li, L. B.; Yang, C. L. Macromolecules 2009, 42, 4751.
46. An, H. N.; Zhao, B. J.; Ma, Z.; Shao, C. G.; Wang, X.; Fang, Y. P.; Li, L. B.; Li, Z. M. Macromolecules 2007, 40, 4740.
47. Lagasse, R. R.; Maxwell, B. Polym Eng Sci 1976, 16, 189.

48. Zuo, F.; Keum, J. K.; Yang, L.; Somani, R. H.; Hsiao, B. S. Macromolecules 2006, 39, 2209.
49. Vleeshouwers, S.; Meijer, H. Rheol Acta 1996, 35, 391.
50. Duplay, C.; Monasse, B.; Haudin, J. M.; Costa, J. L. J Mater Sci 2000, 35, 6093.
51. Li, J. X.; Cheung, W. L.; Jia, D. M. Polymer 1999, 40, 1219.
52. Li, J. X.; Cheung, W. L. J Mater Process Tech 1997, 63, 472.
53. Li, J. X.; Cheung, W. L. Polymer 1998, 39, 6935.
54. Turner-Jones, A.; Alizlewood, J. M.; Beckett, D. R. Macromol Chem 1964, 75, 134.
55. Dragaun, H.; Hubeny, H.; Muschik, H. J Polym Sci Part B: Polym Phys 1977, 15, 1779.
56. Muschik, H.; Dragaun, H.; Skalicky, P. Prog Colloid Polym Sci 1978, 64, 139.
57. Padden, F. J.; Keith, H. D. J Appl Phys 1959, 30, 1479.
58. Yang, L.; Somani, R. H.; Sics, I.; Hsiao, B. S.; Kolb, R.; Fruitwala, H.; Ong, C. Macromolecules 2004, 37, 4845.
59. Somani, R. H.; Yang, L.; Hsiao, B. S.; Sun, T.; Pogodina, N. V.; Lustiger, A. Macromolecules 2005, 38, 1244.
60. Nogales, A.; Hsiao, B. S.; Somani, R. H.; Srinivas, S.; Tsou, A. H.; Balta-Calleja, F. J.; Ezquerra, T. A. Polymer 2001, 42, 5247.
61. Xu, W. B.; Ge, M. L.; He, P. S. J Polym Sci Part B: Polym Phys 2002, 40, 408.
62. Supaphol, P. J Appl Polym Sci 2000, 78, 338.
63. Dukovski, I.; Muthukumar, M. J Chem Phys 2003, 118, 6648.
64. Hu, W.; Frenkel, D.; Mathot, V. B. F. Macromolecules 2002, 35, 7172.
65. Zhang, C.; Hu, H.; Wang, X.; Yao, Y.; Dong, X.; Wang, D.; Wang, Z.; Han, C. C. Polymer 2007, 48, 1105.